Journal of Hazardous Materials 162 (2009) 57–65

Contents lists available at ScienceDirect

Journal of Hazardous Materials

journal homepage: www.elsevier.com/locate/jhazmat

Assessing the airborne titanium dioxide nanoparticle-related exposure hazard at workplace

Chung-Min Liao*, Yu-Hui Chiang, Chia-Pin Chio

Department of Bioenvironmental Systems Engineering, National Taiwan University, Taipei 10617, Taiwan, ROC

ARTICLE INFO

Article history:
Received 5 December 2007
Received in revised form 16 April 2008
Accepted 5 May 2008
Available online 9 May 2008

Keywords:
Titanium dioxide
Nanoparticle
Lung
Risk
Size distribution

ABSTRACT

The purpose of this study was to investigate the effects of size and phase composition on human exposure to airborne titanium dioxide (TiO_2) nanoparticles (NPs) at workplaces. We reanalyzed published data of particle size distribution of airborne TiO_2 NPs during manufacturing activities and linked a physiologically based lung model to estimate size- and phase-specific TiO_2 NP burdens in target lung cells. We also adopted a cell model to simulate the exposure time-dependent size/phase-specific cell uptake of TiO_2 NPs in human dermal and lung cells. Combining laboratory, field, and modeling results, we proposed two major findings: (i) the estimated median effective anatase TiO_2 NP concentration (EC50) for cytotoxicity response on human dermal fibroblasts was estimated to be 24.84 (95% CI: 7.3–70.2) nmol mL^{-1} and EC50 estimate for inflammatory response on human lung epithelial cells was 5414 (95% CI: 3370–7479) nmol mL^{-1} and (ii) packers and surface treatment workers at the TiO_2 NP production workplaces are unlikely to pose substantial risk on lung inflammatory response. Nevertheless, our findings point out that TiO_2 NP production workers have significant risk on cytotoxicity response at relatively high airborne anatase TiO_2 NP concentrations at size range 10–30 nm.

1. Introduction

Nanomaterials are currently being considered for using in modern technology [1,2]. There is, however, a serious lack of information concerning their effect on human health and the environment. Nanoparticles (NPs), which range from 1 to 100 nm in size, are considered to be inhaled and distributed in the body. Inhaled airborne NPs are deposited efficiently in all regions of the respiratory tract. A comprehensive mechanistic understanding has so far been lacking [2–4] but is needed for prediction of airborne NPs on human health effects [5].

Many researches to date had focused on the assessment of atmospheric or inhalation exposures to titanium dioxide (TiO_2) NPs at the workplace [6–9]. International Agency for Research on Cancer (IARC) has recently classified titanium dioxide (TiO_2) as *possibly carcinogenic to human* (Group 2B) [10]. IARC working group concluded that results from studies of inhalation and intratracheal instillation provided sufficient evidence in experimental animals for the carcinogenicity of TiO_2 [11]. National Institute for Occupational and Safety and Health (NIOSH) [12] and IARC [10] also suggested that major epidemiological cohort studies [13–17] had methodological and epidemiological limitations and provided no clear evidence of elevated risks of lung cancer mortality and morbidity among those workers exposed to TiO_2 dust.

Evidence suggests that NPs surface area matters more than particle mass for quantifying lung inflammatory response to NPs exposure and supports the concept that the surface area is the dose measurement that best predicts pulmonary toxicity [18–20]. Limbach et al. [21] indicated that particle size is the most dominant factor than those of primary particle number and total surface area affecting uptake rate of oxide nanoparticles in human lung fibroblasts. Moreover, particle size distribution is inherently more accessible by practical sampling devices for NPs than particle compositions. The published TiO_2 dust exposure data, however, cannot reflect the job- or process-specific particle size distribution effect on lung cancer risk, suggesting that quantification of the job- or process-specific airborne TiO_2 NP size distribution is worth to be considered to assess the internal dose for human exposure [12].

Kang et al. [22] demonstrated that single-walled carbon nanotubes (SWNT) could damage cell membrane and lead to bacterial cell death, implicating plausibly harmful environmental effects. Grassian et al. [7] indicated that mice exposed to TiO_2 NPs with a primary size of 2–5 nm demonstrating a significant but moderate inflammatory response in lung. Sayes et al. [6] indicated that different phase compositions of TiO_2 NPs (e.g., anatase and rutile, or a

* Corresponding author. Tel.: +886 2 2363 4512; fax: +886 2 2362 6433.
E-mail address: cmliao@ntu.edu.tw (C.-M. Liao).

0304-3894/$ – see front matter © 2008 Elsevier B.V. All rights reserved.
doi:10.1016/j.jhazmat.2008.05.020

mixture of the two) affect cytotoxicity and inflammatory response in lung cells. Sayes et al. [6] found that anatase TiO_2 NPs (specific surface area (SSA) = 153 $m^2\,g^{-1}$) was 100 times more toxic than an equivalent sample of rutile TiO_2 (SSA = 123 $m^2\,g^{-1}$), suggesting that oxidative damage in human lung epithelial cells is strongly correlated to crystal phase composition of nanomaterials. Currently, commercial products such as sunscreen and self-cleaning window coating are all consisted of anatase TiO_2 NPs [23,24].

The purpose of this study was to investigate the effects of size and phase composition on human exposure to airborne TiO_2 NPs at workplaces. We reanalyzed published data of particle size distribution of airborne TiO_2 NPs during manufacturing activities. A physiologically based lung model was employed to estimate size- and phase-specific TiO_2 NP burdens in target lung cells. A cell model [25,26] was also adopted to simulate the dynamics of size- and phase-specific cell uptake of TiO_2 NPs in human dermal and lung cells. The proposed cell model was used to describe the uptake dynamics of TiO_2 NPs transporting from cytosol into endosomes and lysosomes. We combined predicted cell TiO_2 NP burdens and reconstructed dose–response profiles to further characterize quantitatively the potential human health risk.

2. Materials and methods

2.1. Quantitative data sources

There is relatively little empirical data regarding airborne TiO_2 NP sources in occupational settings. Accordingly, we must rely on data reanalysis technique together with whatever empirical data is available. TiO_2 NP concentrations and particle size distributions in titanium dioxide plants were obtained from published literature where available by performing a "Web of Science" search (2000–2007), and otherwise from conference papers. Plausible ranges for workplace TiO_2 NP concentrations were defined by the extremes of published values for the given measurements. In this manner, plausible ranges for each job- or process-specific TiO_2 NP exposure concentrations were conservative and included the values from all papers which reported that measured exposure levels. We reanalyzed the measured total TiO_2 NP concentrations through statistical tests.

Our data source search found out that two remarkable datasets related to TiO_2 dust concentrations in titanium dioxide plants, respectively, in the United States (US) [16] and Europe (EU) [17,27], give us the opportunity to test all theoretical considerations of TiO_2 NP exposure effects and quantify its strength. The information of particle size distributions of airborne TiO_2 NPs was obtained from Berges et al. [8] (see Appendix A, Table A1). The information related to the relationship between specific surface area (SSA) and particle diameter of anatase and rutile TiO_2 also collected from recently published data to establish the dosimetric model (see Appendix A, Table A2).

Fryzek et al. [16] collected nearly 2400 separate records of airborne sampling data from 1976 to 2000 for a wide variety of substances such as sulfuric acid mist, sulfur dioxide, hydrogen sulfide, hydrogen chloride, chloride, $TiCl_4$, and TiO_2 that obtained from the four TiO_2 manufacturers. Fryzek et al. [16] then identified 914 air samples for total TiO_2 dust that used in their analysis to estimate relative exposure levels among jobs titles during various time periods. Boffetta et al. [27] collected respirable TiO_2 dust exposure data from 15017 workers employed in 11 pigment-grade TiO_2 production factories in EU from Finland, France, Germany, Italy, Norway, and United Kingdom based on the periods ranging from 1927 to 1969 until 1955 to 2001. Job categories divided into surface treatment including drying, packing, and blending, maintenance mechanics, mixed jobs, and other jobs.

Fryzek et al. [16] indicated that packers, micronizers and addbackes had the highest TiO_2 exposure levels measuring $6.2 \pm 9.4\,mg\,m^{-3}$. Boffetta et al. [27] indicated that workers employed in the surface treatment area had the highest yearly cumulative exposure of 7.75 (interquartile range: 3.24–24.9) $mg\,m^{-3}$. Berges et al. [8] revealed that at the bin filling station in a TiO_2 NP production factory the total number concentrations ranged from 15,000 to 156,000 particles cm^{-3} appeared (range 14–673 nm) with maxima varying between 20 and 30 nm particle diameter compared to the 13,000 particles cm^{-3} outside the plant. Their measurements also indicated that the inhalable dust concentration at the bin filling station was 0.232 $mg\,m^{-3}$, whereas the respirable dust concentration was 0.10–0.141 $mg\,m^{-3}$. These values all exceed the recommended time-weighted average (10-h TWA) concentrations of 1.5 and 0.1 $mg\,m^{-3}$, respectively, for fine and nano-TiO_2 suggested by NIOSH [12].

There are multiple potential sources of variability and uncertainty to be considered during distribution development for TiO_2 NP concentrations in manufacturing plants from measured values. Therefore, data were log-transformed when necessary to meet the assumptions of statistical tests.

2.2. Lung-cellular uptake model

We used a compartmentalized physiologically based (PB) lung model developed by Tran et al. [28–30] and Kuempel et al. [31] to estimate TiO_2 burden in lung tissue. The PB lung model is capable of describing the progress over time of the retention of particles and the alveolar macrophage (AM)-mediated clearance process in the pulmonary region associated with the particle redistribution and the overload phenomena.

The PB lung model mainly divides the lung into three regions of alveolar surface, interstitium, and lymph nodes (Fig. 1A). The alveolar surface region contains four compartments (Fig. 1B): one for incoming free particles (X_1) and the other three represent mobile AMs (X_2), decayed/inactive AMs (X_3), and alveolar sequestration (X_4), respectively. On the other hand, there are also four compartments assigned for interstitium region (Fig. 1C): one for free particles (X_5) and the other three respectively denote mobile interstitial macrophages (IMs) (X_6), decayed/inactive IMs (X_7), and interstitial granuloma (X_8). From the interstitium region, some particles of free and inside IMs can be removed to the lymph nodes region that is represented by compartment X_9 (Fig. 1D). Tran et al. [30] have comprehensively described the PB lung model framework and the essential model parameters that characterizing the model structure and function. A set of ordinary differential equations (Eqs. (1)–(9)) can be reformulated based on Tran et al. [30] with new parameter groupings to describe the dynamic behavior of PB lung model (Table 1).

A cellular uptake model developed by Moore and Allen [26] was adopted to estimate the TiO_2 NP uptake in human dermal fibroblasts and lung epithelial cells (Fig. 1D). The cell model consists of three major compartments, endosome (X_{10}), lysosome (X_{11}), and cytoplasm (X_{12}), describing the uptake processes of TiO_2 NPs (Fig. 1D). Here, we reasonable assumed that lymph nodes burden of TiO_2 NPs could translocate to dermal fibroblasts by lymph circulation systems [19].

The governing equations of the cell model are given in Table 1 (Eqs. (10)–(12)). Table 2 summarizes the lung physiological parameters and rate constants used in cell model along with their likely values employed in the PB lung and cell models. The PB lung-cellular uptake model simulation was performed by the Berkeley

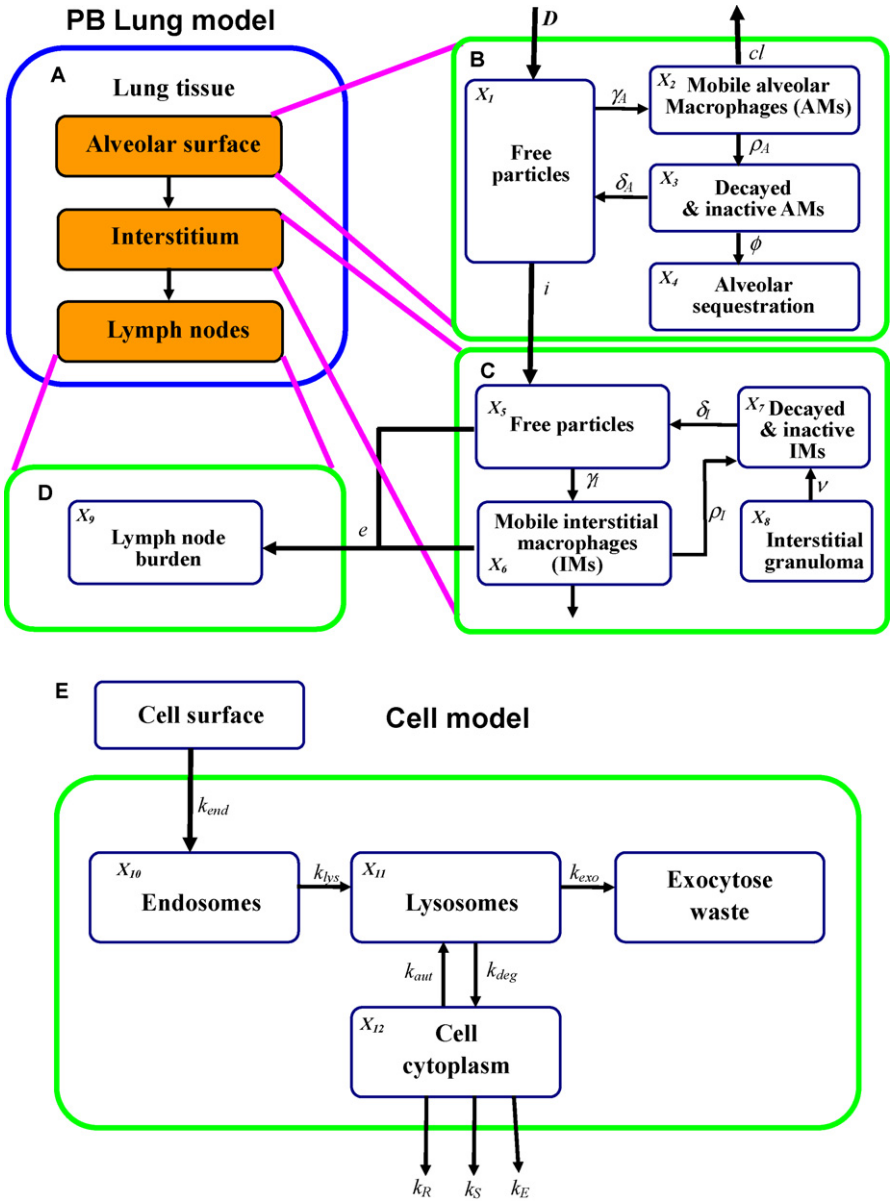

Fig. 1. Schematic representation of proposed compartmentalized physiologically based lung model and cellular uptake model. (A) lung tissue; (B) alveolar surface; (C) interstitum; (D) lymph nodes; and (E) cellular uptake model.

Madonna: Modeling and Analysis of Dynamic Systems (Version 8.3.9, http://www.berkeleymadonna.com).

2.3. Dose–response analysis

Here, we used a three-parameter Hill equation model that is commonly used in pharmacodynamic modeling to optimal fit the experimental data to reconstruct dose–response profiles taking into account the TiO_2 NP effects on human dermal fibroblasts (HDFs) human lung epithelial cells (A594 cells). The well-analyzed related data points from Sayes et al. [6] were appropriately and carefully selected. They used cellular viability as the cytotoxicity endpoint, whereas production of an inflammatory mediator (interleukin-8 (IL-8)) representing inflammatory response endpoint. Their results demonstrated that anatase TiO_2 NPs produced the greater toxicity than that of rutile TiO_2 NPs, revealing that anatase TiO_2 NPs exhibited significant dose–response behavior on cellular viability and human IL-8 response.

Hill equation model captures the relation between lung TiO_2 burden and effect as

$$E = \frac{E_{\max}}{(1 + (\mathrm{EC50}/C)^n)}, \tag{13}$$

where C is the TiO_2 NP concentration ($\mu g\,mL^{-1}$), $E_{\max}$ is the maximum dose effect, EC50 is the concentration that causes an equal effect to half of the $E_{\max}$, and n is a slope factor referred to as the Hill coefficient determining the overall shape of the curve. Hill coefficient is a measure of cooperativity. A value of $n > 1$ indicates positive cooperativity.

2.4. Risk characterization

Risk at a specific target organ concentration C, can be calculated as the proportion of the group expected to have that tissue concentration multiplied by the conditional probability of adverse effects, given concentration C. This results in a joint probability function or

Table 1
Equations used in the PB lung and cellular uptake models[a]

Alveolar surface

$$\frac{dX_1}{dt} = D - r_A X_1 - [i_{normal}\theta(S_{alv}) + (1-\theta(S_{alv}))i_{max}]X_1 + \theta(S_{alv})\delta_A X_3 \quad (1)$$

$$\frac{dX_2}{dt} = r_A X_1 - \theta(S_{alv})clX_2 - \rho_A X_2 \quad (2)$$

$$\frac{dX_3}{dt} = \rho_A X_2 - \theta(S_{alv})\delta_A X_3 - (1-\theta(S_{alv}))\phi X_3 \quad (3)$$

$$\frac{dX_4}{dt} = (1-\theta(S_{alv}))\phi X_3 \quad (4)$$

Interstitium

$$\frac{dX_5}{dt} = [i_{normal}\theta(S_{alv}) + (1-\theta(S_{alv}))i_{max}]X_1 - \theta(S_{inst})eX_5 - \gamma_I X_5 + \theta(S_{inst})\delta_I X_7 \quad (5)$$

$$\frac{dX_6}{dt} = \gamma_I X_5 - \rho_I X_6 - \theta(S_{inst})eX_6 \quad (6)$$

$$\frac{dX_7}{dt} = \rho_I X_6 - \theta(S_{inst})\delta_I X_7 - (1-\theta(S_{inst}))\nu X_7 \quad (7)$$

$$\frac{dX_8}{dt} = (1-\theta(S_{inst}))\nu X_7 \quad (8)$$

Lymphatic nodes

$$\frac{dX_9}{dt} = \theta(S_{inst})e(X_5 + X_6) \quad (9)$$

Cellular uptake

$$\frac{dX_{10}}{dt} = k_{end}X_9 - k_{lys}X_{10} \quad (10)$$

$$\frac{dX_{11}}{dt} = k_{lys}X_{10} + k_{aut}X_{12} - (k_{exo} + k_{deg})X_{11} \quad (11)$$

$$\frac{dX_{12}}{dt} = k_{deg}X_{11} - (k_{aut} + k_R + k_S + k_E)X_{12} \quad (12)$$

[a] Abbreviations and parameter symbols: D: deposited dose rate ($m^2\ day^{-1}$); r_A: phagocytosis rate by alveolar macrophage (AM) (day^{-1}); i_{normal}: normal interstitialisation rate of particle (day^{-1}); i_{max}: maximum interstitialisation rate of particle (day^{-1}); $\theta(S_{alv})$: function of alveolar surface burden that describe retardation of clearance of insoluble dust; δ_A: rate of particles back to alveolar surface for rephagocyosis (day^{-1}); ρ_A: transfer rate of particles from active to inactive AMs (day^{-1}); cl: AM-mediated clearance of particle (day^{-1}); ϕ: alveolar sequestration (day^{-1}); $\theta(S_{inst})$: function of interstitium burden that describe retardation of clearance of insoluble dust; e: removal rate of particles to lymph nods; r_I: phagocytosis rate by interstitial macrophage (IM) (day^{-1}); δ_I: rate of particles back to interstitium for rephagocyosis (day^{-1}); ρ_I: transfer rate of particles from active to inactive IMs (day^{-1}); ν: rate of formation of interstitial granuloma (day^{-1}); k_{end}: rate constant of endocytosis (min^{-1}); k_{lys}: the rate constant of lysosoma (min^{-1}); k_{deg}: rate constant of intracellular digestion; k_{aut}: the rate constant of autophagy; k_{exo}: rate constant of exocytosis; k_R: rate constant of respiration; k_S: rate constant of secretion; and k_E: rate constant of export.

exceedance risk profile as

$$R_C = P(C)P(E|C), \quad (14)$$

where R_C is the risk at a specific concentration C, $P(C)$ is the probability of having tissue concentration C, and $P(E|C)$ is the conditional probability of the adverse effect, given tissue concentration C.

The overall expected risk for job-specific workers might be computed as the sum of the risks given the most possible prevalent exposure routes [32],

$$R = \int_{-\infty}^{\infty} 1/(\sqrt{2\pi}\sigma_e)\exp\left[-1/2\left(\frac{(\log C - \mu_e)}{\sigma_e}\right)^2\right] \times P(E|C)\mathrm{d}\log C, \quad (15)$$

where μ_e and σ_e are mean and standard deviation of the log-transformed TiO_2 exposures, respectively; and R is the estimated fraction of the job-specific workers that is expected to suffer adverse effects.

2.5. Uncertainty analysis

Capturing uncertainty is a key element in risk assessment. Uncertainty arises from estimation of both exposure and effects. In order to quantify this uncertainty and its impact on the estimation of expected risk, a Monte Carlo (MC) simulation that includes input distributions for the parameters of the derived concentration–response function as well as for estimated exposure parameters was implemented. Ten thousand executions of the MC simulation were performed. A 95% confidence interval (CI) for expected risk was determined on the basis of the 2.5th and 97.5th quantiles of the simulation results. A risk curve was generated from the cumulative distribution of simulation outcomes. The statistical analyses and simulations were implemented using Crystal Ball software (Version 2000.2, Professional Edition, Decisioneering, Inc., Denver, CO, USA).

Table 2
Input parameters used in PB lung and cellular uptake models (see Table 1 for the symbol meanings)

Symbols	Unit	Value
Alveolar surface[a]		
r_A	day^{-1}	0.966
i_{normal}	day^{-1}	0.0072
i_{max}	day^{-1}	0.4347
$\theta(S_{alv})$	–	0.6
δ_A	day^{-1}	0.14
ρ_A	day^{-1}	0.036
cl	day^{-1}	0.0036
ϕ	day^{-1}	0.14
Interstitium[a]		
r_I	day^{-1}	0.966
$\theta(S_{inst})$	–	0.6
δ_I	day^{-1}	0.14
ρ_I	day^{-1}	0.036
ν	day^{-1}	0.14
Lymph nodes[a]		
e	day^{-1}	0.0242
Cellular uptake[b]		
k_{end}	$L\,min^{-1}\,cell^{-1}$	1.4×10^{-15}
k_{lys}	$L\,min^{-1}\,cell^{-1}$	2.72×10^{-15}
k_{deg}	$L\,min^{-1}\,cell^{-1}$	7.48×10^{-15}
k_{aut}	$L\,min^{-1}\,cell^{-1}$	8.28×10^{-15}
k_{exo}	$L\,min^{-1}\,cell^{-1}$	7.48×10^{-15}
k_R	$L\,min^{-1}\,cell^{-1}$	2.72×10^{-17}
k_S	$L\,min^{-1}\,cell^{-1}$	1.99×10^{-18}
k_E	$L\,min^{-1}\,cell^{-1}$	8.16×10^{-16}

[a] Adopted from Tran et al. [30].

[b] The rate constants used in cellular uptake model were calculated from cell volume ratio between mussels and human lung fibroblasts as: $k_{hf\,cell} = (V_{hf\,cell}/V_{m\,cell}) \times k_{m\,cell}$ where $V_{hf\,cell}$ is the cell volume of human lung fibroblasts ($V_{hf\,cell} = 1.8\times10^{-12}$ L [21]); $V_{m\,cell}$ is the cell volume of mussels ($V_{m\,cell} = 1.32\times10^{-12}$ L [26]); $k_{m\,cell}$ is the rate constant of cell of mussel adopting from Moore and Allen [26]; and $k_{hf\,cell}$ is the present calculated rate constant.

3. Results

3.1. TiO_2 NPs size distribution and dosimetric model

We best fitted the lognormal probabilistic model ($r^2 = 0.95$) to pooled particle size distribution data during filling operation of TiO_2 NPs [8], resulting in a geometric mean (gm) of 24.81 nm with a geometric standard deviation (gsd) of 1.38 (Fig. 2A). On the other hand, the best fitted model ($r^2 = 0.91$) for outside atmospheric environment of factory followed a lognormal distribution with a gm 42.71 nm and a gsd 1.45 (Fig. 2B).

The dosimetric models describing the SSA and particle diameter (d_p) relations of TiO_2 NPs were reconstructed. Our results indicate that a linear model of $\ln Y = 6.12 - 0.56\ \ln X$ ($r^2 = 0.90$, $n = 8$) best describe SSA–d_p profile for anatase TiO_2 (Fig. 3A), whereas SSA–d_p profile for rutile TiO_2 is best described by $\ln Y = 5.52 - 0.46\ \ln X$ ($r^2 = 0.91$, $n = 9$) (Fig. 3B).

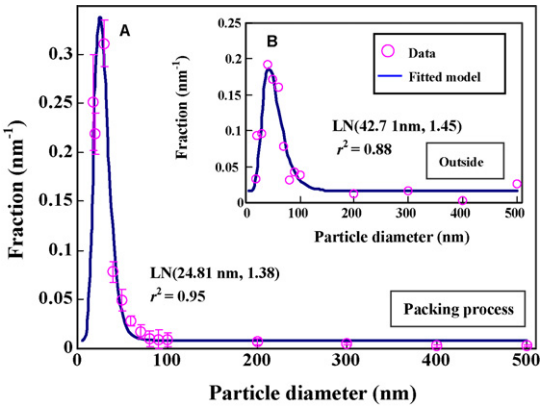

Fig. 2. Size distribution of TiO_2 particles during filling operation at workplace for (A) packing process and (B) outside of workplace. Error bar represents the standard deviation from mean (n = 4).

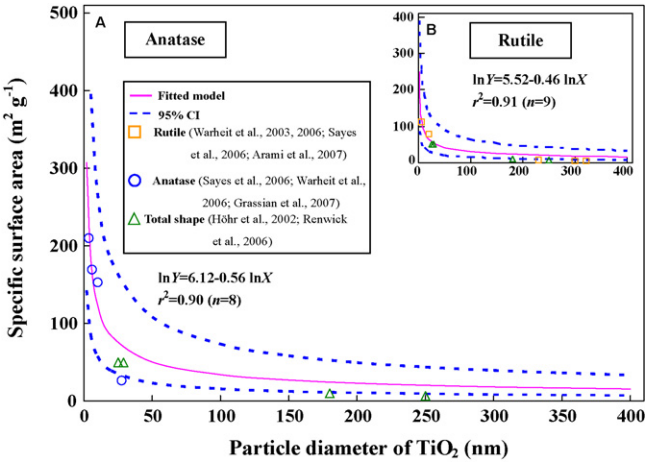

Fig. 3. Reconstructed dosimetric models describing the relationship between specific surface area and particle diameter of TiO_2 NPs for (A) anatase and (B) rutile. Data sources were adopted from published literature [6,7,35,39–42].

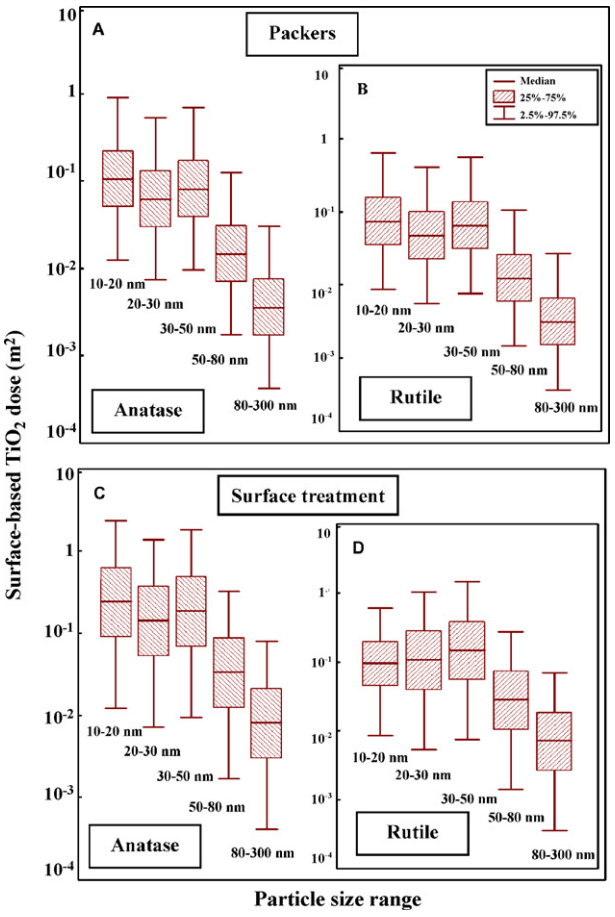

Fig. 4. Box and whisker representations of different particle size ranges of specific surface area-based airborne anatase and rutile TiO_2 NP concentrations in TiO_2 production work setting for (A) packers and (B) surface treatment workers.

3.2. Exposure assessment

In order to well define the size distribution of TiO_2 particles, five size categories were divided with the particle diameter, 10–20, 20–30, 30–50, 50–80, and 80–300 nm, accounting for the percentage of overall particles of 25.09, 21.86, 38.36, 9.50, and 2.90%, respectively, based on the fitted particle size distribution (Fig. 2A). We appropriately log-transformed the original data obtained from Fryzek et al. [16] and Boffetta et al. [17] to surface area-based TiO_2 NP concentrations, resulting in 0.1685 (95% CI: 0.02–1.45) m^2 for packers and 0.387 (0.02–3.74) m^2 for surface treatment workers. A conversion factor of particle percentage (%) × mass concentration (mg m^{-3}) × V (m^3) × SSA (m^2 g^{-1}) × 10^{-3} (g mg^{-1}) is used to estimate size range-specific surface area dose where V is the working space volume (here we reasonably assume V = 300 m^3) (Table 3).

Fig. 4 gives the size range-specific surface area-based airborne anatase and rutile TiO_2 NP doses for packers and surface treatment workplaces. Our results indicate that packers were exposed to higher median surface area-based airborne anatase TiO_2 NP doses of 0.081–0.105 m^2 for d_p ranging from 10 to 50 nm (Fig. 4A), whereas 0.065 to 0.074 m^2 for rutile TiO_2 NP doses (Fig. 4B). On the other hand, for d_p 10–50 nm, surface treatment workers were subjected to median airborne TiO_2 NP doses ranging from 0.187 to 0.241 m^2 for anatase and 0.095 to 0.148 m^2 for rutile (Fig. 4C and D).

Fig. 5 demonstrates bin-specific lung anatase and rutile TiO_2 NP burdens in lung surface area and in interstitial granuloma for

Table 3
Size range-specific percentage of particles, mass concentration, and estimated specific surface area for anatase and rutile TiO_2 NPs

Particle size range (nm)	Percentage of particles (%)[a]	Mass concentration[b] (mg m^{-3})		Specific surface area (SSA)[c] (m^2 g^{-1})	
		Packer	Surface treatment	Anatase	Rutile
10–20	25.09	0.85	1.94	124.27	86.98
20–30	21.86	0.74	1.69	84.13	63.25
30–50	38.36	1.31	3.01	61.97	49.25
50–80	9.50	0.32	0.73	45.72	38.41
80–300	2.90	0.1	0.23	36.22	31.81

[a] Adopted from Berges et al. [8] and the original data we obtain from table S1.
[b] The data of Packer adopted from Fryzek et al. [16] and the data of surface treatment adopted from Boffetta et al. [27].
[c] We adopted the SSA–d_p data of TiO_2 from table S2 and used these data to fit the relation of SSA–d_p.

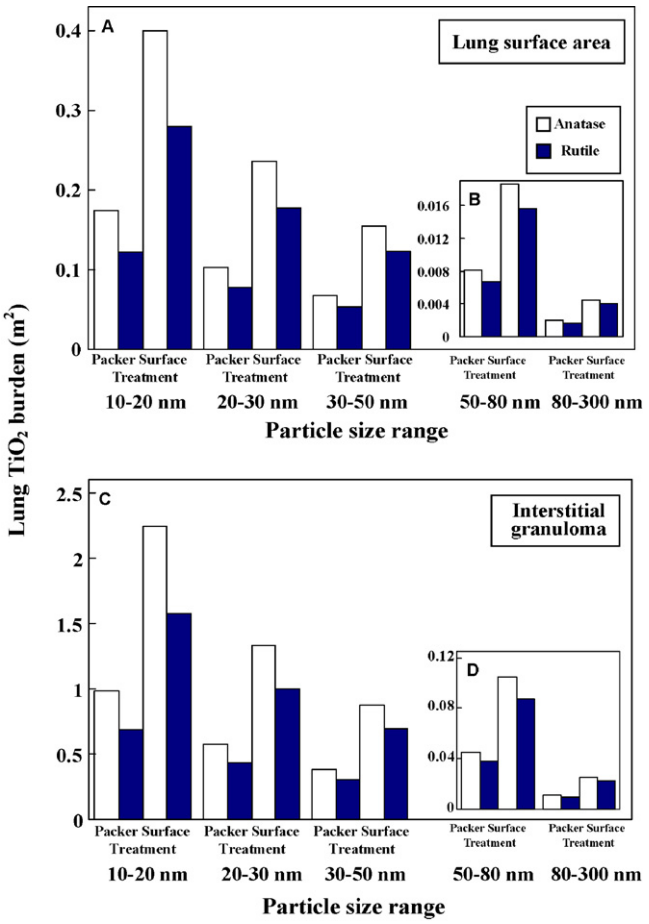

Fig. 5. Lung anatase and rutile TiO_2 NP burdens varied with different particle size ranges in (A and B) lung surface area and (C and D) in interstitisl granuloma.

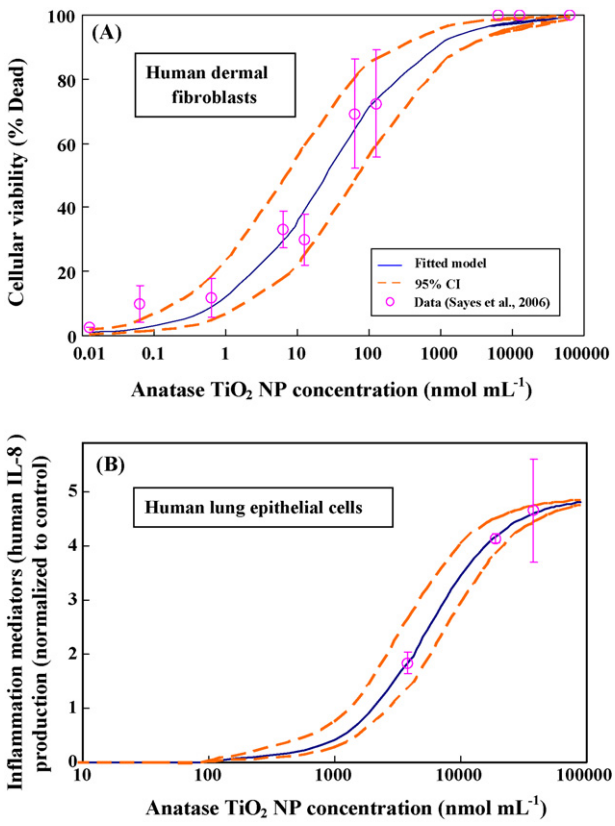

Fig. 6. Reconstructed Hill model-based dose–response profiles for (A) TiO_2-induced cellular viability for human dermal fibroblasts and (B) lung inflammatory mediators production for human lung epithelial cells.

packers and surface treatment workers. Our results show that the highest TiO_2 NP burdens in lung surface area of packers were estimated to be 0.174 m^2 (anatase) and 0.122 m^2 (rutile) for d_p at 10–20 nm compared to 0.002 m^2 (anatase) and 0.0017 m^2 (rutile) in d_p range 80–300 nm (Fig. 5A and B). In view of Fig. 5A and B, surface treatment workers were subjected to a relative higher TiO_2 NP burdens in lung surface area than those of packers, indicating that 0.40 m^2 (anatase) and 0.28 m^2 (rutile) for d_p 10–20 nm. On the other hand, TiO_2 NP burdens in interstitial granuloma yielded a higher TiO_2 NP burdens than that of in lung surface area (Fig. 5). Surface treatment workers appeared to be having higher TiO_2 NP burdens in interstitial granuloma (2.248 m^2 (anatase) and 1.574 m^2 (rutile) for d_p at 10–20 nm) compared to that of packers (0.98 m^2 (anatase) and 0.686 m^2 (rutile)) (Fig. 5C).

3.3. Dose–response assessment

The reconstructed Hill-based TiO_2 dose–response profiles are shown in Fig. 6. The Hill equation model and a 10,000 MC simulation provide an adequate fit for the experimental data [6] from pooled anatase TiO_2 NPs on cellular viability ($r^2 = 0.93$) (Fig. 6A) and inflammatory response expressed by human IL-8 production ($r^2 = 0.89$) (Fig. 6B). The median effective anatase TiO_2 NP concentration (EC50) for cellular viability was estimated to be 24.84 (95% CI: 7.3–70.2) nmol mL^{-1} and EC50 estimate for human IL-8 production was 5414 (95% CI: 3370–7479) nmol mL^{-1}. The fitted Hill coefficients (n) were estimated to be 1.03 for anatase TiO_2 NP-cellular viability effect and 1.40 for anatase TiO_2 NP-inflammatory response effect.

3.4. Cellular uptake and risk estimates

Simulation of cellular uptake of anatase TiO_2 NPs in lung surface area and lymph nodes, made it possible to better understand the processes governing TiO_2 NP transport in human cells (Fig. 7). Fig. 7 indicates that the lung surface area and lymph nodes were uptake anatase TiO_2 NPs linearly and exponentially, respectively. Fig. 7A depicts that endosomes suffered the largest uptake amounts of anatase TiO_2 NPs of particle sizes ranging from 10 to 20 nm (2184.95 nmol mL^{-1} at day 12) and followed the order of 20–30 nm (1411.72 nmol mL^{-1}), 30–50 nm (1229.63 nmol mL^{-1}), and 50–80 nm (528.98 nmol mL^{-1}). Likewise, the endosomes compartment in lymph nodes (Fig. 7C) shows the similar uptake patterns to those of in lung surface cells, showing that the size range-specific uptake levels of anatase TiO_2 NPs also followed the order of 10–20 nm (124.47 nmol mL^{-1}), 20–30 nm (80.42 nmol mL^{-1}), 30–50 nm (70.05 nmol mL^{-1}), and 50–80 nm (30.14 nmol mL^{-1}). No significant cellular uptake levels of anatase TiO_2 NPs appeared in lysosomes compartment for lung surface area and lymph nodes in that the uptake concentrations ranged from 10^{-13} to 10^{-11} nmol mL^{-1} (Fig. 7B and D).

Risk curves for the anatase TiO_2 NPs-induced inflammation response on human lung epithelial cells (Fig. 8A and B) indicate that the risk = 0.5 at workplace, the normalized human IL-8 production were estimated to be 0.66 (95% CI: 0.44–1.15) for 10–20 nm and 0.43 (0.28–0.77) for 20–30 nm. This result suggests that packers and surface treatment workers at the TiO_2 NP production workplaces are unlikely to pose substantial risk on lung inflammatory

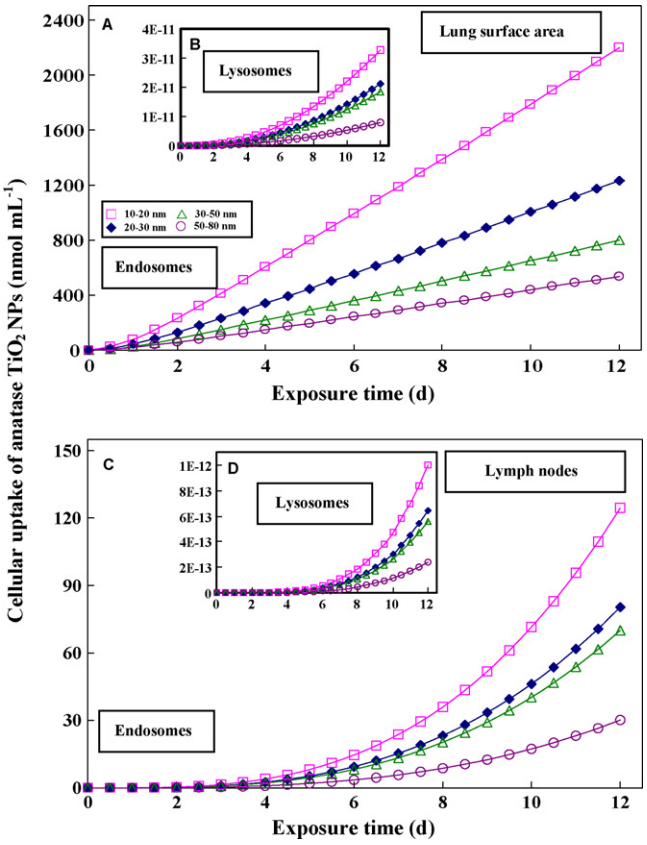

Fig. 7. Lysosmes and lysosomes uptake of anatase TiO_2 NPs in the cells of (A and B) lung surface area and (C and D) lymph nodes.

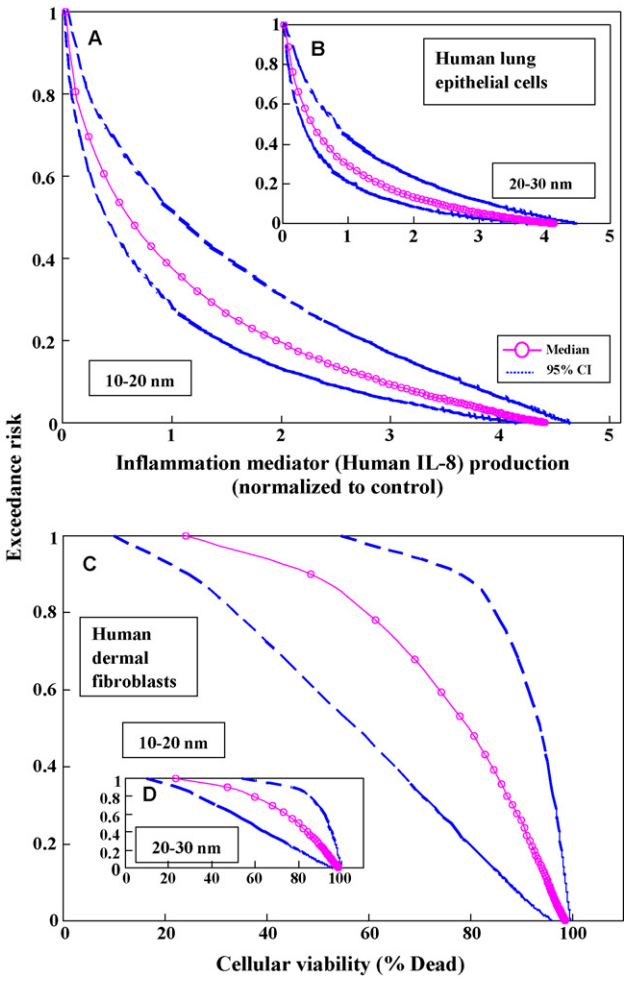

Fig. 8. Estimated exceedance risk curves with 95% CI for (A and B) human lung epithelial cells and (C and D) human dermal fibroblasts varied with particle size ranges of 10–20 and 20–30 nm for surface treatment workers.

response. On the other hand, at least 80.76% (95% CI: 59.18–94.03%) for 10–20 nm and 79.88% (95% CI: 57.81–93.71%) for 20–30 nm of anatase TiO_2 NPs having 50% probability rendered human dermal fibroblasts suffering cytotoxicity responses (Fig. 8C and D). Fig. 8C and D thus indirectly indicate that TiO_2 NP production workers such as packers and surface treatment have significant risk on cytotoxicity response at relatively high airborne anatase TiO_2 NP concentrations at size range 10–30 nm. Table 4 summarizes the size range-specific exceeding thresholds for the probabilities of cytotoxicity and inflammatory responses at risk = 0.2, 0.5, and 0.8 for TiO_2 production workers of packers and surface treatment in workplaces exposed to airborne TiO_2 NPs.

4. Discussion

4.1. Lung-cellular uptake model

This work represents, to our knowledge, the first systematic evaluation in assessing the potential inhalation risk at workplace of TiO_2 NPs production factories. We evaluated the effects of particle size distribution and phase composition of TiO_2 NPs on exposure hazard. The Hill model was used to reconstruct dose–response profiles based on data of anatase TiO_2 NPs on human dermal fibroblasts and human lung epithelial cells to respectively correlate cytotoxicity and inflammatory responses. The PB lung model was employed to estimate job- and particle size range-specific surface area-based TiO_2 burdens in alveolar surface and interstitial granuloma, respectively. A cell model was applied to predict size range-specific cellular uptake of anatase TiO_2 NPs, estimating the likelihood of risk characterized by cytotoxicity and inflammatory responses.

Combining laboratory, field, and modeling results, we proposed two major findings to the current studies: (i) the estimated median effective anatase TiO_2 NP concentration (EC50) for cytotoxicity

Table 4
Probability of human lung inflammatory and dermal cytotoxicity responses for TiO_2 NP production workers exceeding threshold (median with 95% CI)

Particle size range (nm)	Exceedance risk					
	Inflammatory response, human IL-8 production			Cytotoxicity response, cell viability (%dead)		
	0.8	0.5	0.2	0.8	0.5	0.2
10–20	0.12 (0.08–0.23)	0.66 (0.44–1.15)	1.96 (1.46–2.77)	70.28 (37.34–98.1)	77.96 (59.18–94.03)	91.61 (77.96–97.46)
20–30	0.15 (0.11–0.29)	0.43 (0.28–0.77)	1.5 (1.07–2.27)	63.2 (37.25–95.6)	79.88 (57.81–93.71)	91.64 (79.09–97.63)
30–50	0.11 (0.07–0.21)	0.38 (0.25–0.69)	1.3 (0.92–2.03)	37.76 (16–61.24)	66.22 (40.36–88.03)	85.82 (67.63–95.78)
50–80	0.03 (0.02–0.06)	0.12 (0.07–0.22)	0.49 (0.33–0.88)	42.53 (20.35–73.5)	46.88 (23.35–76.8)	71.62 (46.56–90.45)

response on human dermal fibroblasts was estimated to be 24.84 (95% CI: 7.3–70.2) nmol mL^{-1} and EC50 estimate for inflammatory response on human lung epithelial cells was 5414 (95% CI: 3370–7479) nmol mL^{-1} and (ii) the size range-specific risk curves (Fig. 8) are the pivotal results for public policy.

Fryzek et al. [16] and Boffetta et al. [17] both suggested that the workers exposures in US and EU TiO_2 production factories were not associated with a carcinogenic effect of TiO_2 dust on the human lung based on a cohort mortality epidemiological study. NIOSH [12], however, indicated that these epidemiological studies may have lacked the statistical strength to test an increased risk of mortality from TiO_2-associated pneumoconiosis. Our proposed risk analysis may compensate this disadvantage by using a scientifically based framework for the risk assessment for the TiO_2 NPs that may be encountered at the workplaces. Generally, our results show that packers and surface treatment workers at the TiO_2 NP production workplaces are unlikely to pose substantial risk on lung inflammatory response. Nevertheless, our findings point out that TiO_2 NP production workers have significant risk on cytotoxicity response at relatively high airborne TiO_2 anatase NP concentrations at size 10–30 nm.

4.2. Effects of particle size and phase composition of TiO_2 NPs

It has been widely demonstrated that particle size, degree of agglomeration, specific surface area, phase composition, and number concentration may affect NP uptake [6,19,21,33,34]. Limbach et al. [21] revealed that oxide NP uptake in human lung fibroblasts was stronger dependent on particle size than those of number density or total particle surface area. However, pulmonary toxicology studies with nanoscale TiO_2 rods and dots in rats indicated that toxicity may not be dependent upon particle size and surface area [35].

Our results show that cellular uptake of anatase TiO_2 NPs increases linearly and exponentially, respectively, in the particle diameter size range of 10–30 nm (Fig. 7). This indicates that particle number within specific particle size ranges may be important. Suzuki et al. [36] revealed that TiO_2 NPs easily moved to the cytoplasm of the mammalian cells, not to the nucleus and were taken up in the cells depending on the NP dose, reactive time, and particle size. Anatase TiO_2 NPs of 10–30 nm in size are potentially highly mobile because of their small size. Agglomeration, however, may restrict TiO_2 NP transport by inducing settling, and it can drive crystal growth, leading to decreased solubility and further in limiting NP dispersal in human cells.

4.3. Limitations and implications

We recognized limitations in each of our data sources, particularly the inherent problem of uncertainty and variability of the data. The strength of these results rests on the robustness of the proposed Hill-PB lung model as well as cell model and the public and regulatory authorities' guideline values. Nevertheless, our analysis may provide a wider context for the interpretation of regional TiO_2 NPs-related inhalation risk profiling that produced diverging and controversial outcomes, which has economic and policy implications. Although more complex models may be necessary to answer specific questions regarding risk or particular management strategies, our simple model captures the essential risk analysis methodology and it is flexible enough to integrate effects occurring at varying job- or process- and particle size-specific scales at workplace.

Our results have several implications. First, our results suggest that potential particle size-related health risk following inhalation exposure to occupational nanoaerosols that is appropriately reflected by surface area associated with particle number within a specific particle size range. Second, our approach should have certain advantages over methods for dose response profiles selection that are dependent on the use of TiO_2 NPs on hazard-based toxicity studies to characterize particular aspects of risk analysis. The proposed compartmental modeling can be used to show that the primary advantage of targeted TiO_2 NPs is associated with processes involved in cellular uptake in target cells. Moreover, linking Hill model-based dose–response relationships and PB lung-cell uptake model has an important theoretical advantage over traditional models. It can potentially take account of both physiological and occupational factors affecting TiO_2 NP-related adverse health responses [37,38].

Last, our results show that packers might have potential risk on dermal exposure at relatively high airborne anatase TiO_2 NP concentrations at size range 10–30 nm. Reduce in direct skin contact from TiO_2 NPs that decrease the frequency of dermal exposure could provide level of protection at the workplace.

Appendix A

Tables A1 and A2.

Table A1
Original data of particle numbers of TiO_2[a]

Particle diameter (nm)	Sampling time inside: filling operation				Outside 09:26
	10:27	10:41	11:39	11:42	
18	91000	630000	21000	50000	9100
20	88000	510000	22000	70000	26000
30	480000	400000	52000	50000	27000
40	110000	106000	21000	10000	54000
50	76000	51000	20000	9200	48000
60	48000	23000	9700	9000	45000
70	23000	16000	8600	5500	22000
80	9800	9400	7900	5800	8800
90	7700	7400	7500	7500	12000
100	7800	7900	8000	5200	10900
200	1200	5000	7400	7400	3600
300	830	4100	7400	2400	4600
400	270	680	780	6900	760
500	760	630	730	6700	7400
600	–	640	750	–	840

[a] Adopted from Berges et al. [8].

Table A2
Original data of the relationship between different shape of TiO_2 and corresponding specific surface area

Crystal phase	Particle diameter (nm)	SSA ($m^2\ g^{-1}$)[a]	Reference
Rutile	320	6	Warheit et al. [39]
	300	6	Warheit et al. [35]
	230	8.2	Warheit et al. [39]
	20	78.88	Arami et al. [40]
	5.2 ± 0.65[b]	112	Sayes et al. [6]
Anatase	20–35 (27.5)[c]	26.5	Warheit et al. [35]
	10.1 ± 1	153	Sayes et al. [6]
	5.8–6.1 (5.95)	169.4	Warheit et al. [35]
	3.5 ± 1	210 ± 10	Grassian et al. [7]
Total shape	250	6.6	Renwick et al. [42]
	29	49.78	Renwick et al. [42]
	180	10	Höhr et al. [41]
	20–30 (25)	50	Höhr et al. [41]

[a] SSA denotes specific surface area.
[b] Mean ± S.D.
[c] Min–max (median).

References

[1] R.D. Handy, B.J. Shaw, Toxic effects of nanoparticles and nanomaterials: implications for public health, risk assessment and the public perception of nanotechnology, Health Risk Soc. 9 (2007) 25–144.
[2] R. Owen, R. Handy, Formulation the problems for environmental risk assessment of nanomaterials, Environ. Sci. Technol. 41 (2007) 5582–5588.
[3] A.D. Maynard, R.J. Aitken, T. Butz, V. Colvin, K. Donaldson, G. Oberdörster, M.A. Philbert, J. Ryan, A. Seaton, V. Stone, S.S. Tinkle, L. Tran, N.J. Walker, D.B. Warheit, Safe handling of nanotechnology, Nature 444 (2006) 267–269.
[4] A.D. Maynard, R.J. Aitken, Assessing exposure to airborne nanomaterials: current abilities and future requirements, Nanotoxicology 1 (2007) 26–41.
[5] J.M. Balbus, K. Florini, R.A. Denison, S.A. Walsh, Protecting workers and the environment: an environmental NGO's perspective on nanotechnology, J. Nanopart. Res. 9 (2007) 11–22.
[6] C.M. Sayes, R. Wahi, P.A. Kurian, Y. Liu, J.L. West, K.D. Ausman, D.B. Warheit, V.L. Colvin, Correlating nanoscale titania structure with toxicity: a cytotoxicity and inflammatory response study with human dermal fibroblasts and guman lung epithelial cells, Toxicol. Sci. 92 (2006) 174–185.
[7] V.H. Grassian, P.T. O'Shaughnessy, A. Adamcakova-Dodd, J.M. Pettibone, P.S. Thorne, Inhalation exposure study of titanium dioxide nanoparticles with a primary particle size of 2 to 5 nm, Environ. Health Perspect. 115 (2007) 397–402.
[8] M. Berges, C. Möhlmann, B. Swennen, Y.V. Rompaey, P. Berghmans, Workplace exposure characterization at TiO_2 nanoparticle production, in: Proceedings of the 3rd International Symposium on Nanotechnology, Occupational and Environmental Health, Taipei, Taiwan, 2007.
[9] ISO/TR. Workplace atmospheres-Ultrafine, nanoparticle and nano-strcutured aerosols-inhalation exposure characterization and assessment, Internation Organization for Standardization Technical Report, Swizerland, 2007.
[10] IARC. Titanium dioxide Group 2B, Monographs on the evaluation of carcinogenic risks to humans, International Agency for Research on Cancer, World Health Organization, Lyon, 2006, vol. 9.
[11] R. Baan, K. Straif, Y. Grosse, B. Secretan, F.E. Ghissassi, V. Cogliano, Carcinogenicity of carbon black, titanium dioxide, and talc, Lancet Oncol. 7 (2006) 295–296.
[12] NIOSH. NIOSH current intelligence bulletin: evaluation of health hazard and recommendations for occupational exposure to titanium dioxide, Draft., Department of Health and Human Services. Public Health Service. Centers for Disease Control and Prevention. National Institute for Occupational Safety and Health, DHHS (NIOSH) publication, Cincinnati, 2005.
[13] J.L. Chen, W.E. Fayerweather, Epidemiologic study of workers exposed to titanium dioxide, J. Occup. Environ. Med. 30 (1988) 937–942.
[14] W.E. Fayerweather, M.E. Karns, P.G. Gilby, J.L. Chen, Epidemiologic study of lung cancer mortality in workers exposed to titanium tetrachloride, J. Occup. Environ. Med. 34 (1992) 164–169.
[15] P. Boffetta, V. Gaborieau, L. Nadon, M.E. Parent, E. Weiderpass, J. Siemiatycki, Exposure to titanium dioxide and risk of lung cancer in a population-based study from Montreal, Scand. J. Work Environ. Health 27 (2001) 227–232.
[16] J.P. Fryzek, B. Chadda, D. Marano, K. White, S. Schweitzer, J.K. McLaughlin, W.J. Blot, A cohort mortality study among titanium dioxide manufacturing workers in the United States, J. Occup. Environ. Med. 45 (2003) 400–409.
[17] P. Boffetta, A. Soutar, J.W. Cherrie, F. Granath, A. Andersen, A. Anttila, M. Blettner, V. Gaborieau, S.J. Klug, S. Langard, D. Luce, F. Merletti, B. Miller, D. Mirabelli, E. Pukkala, H.O. Adami, E. Weiderpass, Mortality among workers employed in the titanium dioxide production industry in Europe, Cancer Causes Control 15 (2004) 697–706.
[18] K. Donaldson, V. Stone, C.L. Tran, W. Kreyling, P.J.A. Borm, Nanotoxicology, Occup. Environ. Med. 61 (2004) 727–728.
[19] G. Oberdörster, E. Oberdörster, J. Oberdörster, Nanotoxicology: an emerging discipline evolving from studies of ultrafine particles, Environ. Health Perspect. 113 (2005) 823–839.
[20] K. Wittmaack, In search of the most relevant parameter for quantifying lung inflammatory response to nanoparticle exposure: particle number, surface area, or what? Environ. Health Perspect. 115 (2007) 187–194.
[21] L.K. Limbach, Y. Li, R.N. Grass, T.J. Brunner, M.A. Hintermann, M. Muller, D. Gunter, W.J. Stark, Oxide nanoparticle uptake in human lung fibroblasts: effects of particle size, agglomeration, and diffusion at low concentrations, Environ. Sci. Technol. 39 (2005) 9370–9376.
[22] S. Kang, M. Pinault, L.D. Pfefferle, M. Elimelech, Single-walled carbon nanotubes exhibit strong antimicrobial activity, Langmuir 23 (2007) 8670–8673.
[23] N. Serpone, A. Salinaro, A. Emeline, Deleterious effects of sunscreen titanium dioxide nanoparticles on DNA: efforts to limit DNA damage by particle surface modification, SPIE, Int. Soc. Opt. Eng. 4258 (2001) 86–98.
[24] I.P. Parkin, R.G. Palgrave, Self-cleaning coatings, J. Mater. Chem. 15 (2005) 1689–1695.
[25] M.N. Moore, R.I. Willows, A model for cellular uptake and intracellular behaviour of particulate-bound micropollutants, Mar. Environ. Res. 46 (1998) 509–514.
[26] M.N. Moore, J.I. Allen, A computational model of the digestive gland epithelial cell of marine mussels and its simulated responses to oil-derived aromatic hydrocarbons, Mar. Environ. Res. 54 (2002) 579–584.
[27] P. Boffetta, A. Soutar, E. Weiderpass, J. Cherrie, F. Granath, A. Andersen, A. Anttila, M. Blettner, V. Gaborieau, S. Klug, S. Langard, D. Luce, F. Merletti, B. Miller, D. Mirabelli, E. Pukkala, H.O. Adami, Historical cohort study of workers employed in the titanium dioxide production industry in Europe. Results of mortality follow-up, Final Report, Department of Medical Epidemiology, Karolinska Institutet, Stockholm (2003).
[28] C.L. Tran, A. Jones, R.T. Cullen, K. Donaldson, Mathematical modeling of the retention and clearance of low-toxicity particles in the lung, Inhal. Toxicol. 11 (1999) 1059–1076.
[29] C.L. Tran, D. Buchanan, A.D. Jones, Mathematical modeling to product the response to poorly soluble particle in rat lungs, Inhal. Toxicol. 12 (Suppl 3) (2000) 403–409.
[30] C.L. Tran, A.D. Jones, G.B. Miller, K. Donaldson, Modeling the retention and clearance of manmade vitreous fibers in the rat lung, Inhal. Toxicol. 15 (2003) 553–587.
[31] E.D. Kuempel, C.L. Tran, R.J. Smith, A.J. Bailer, A biomathematical model of particle clearance and retention in the lungs of coal miners. II. Evaluation of variability and uncertainty, Regul. Toxicol. Pharmacol. 34 (2001) 88–101.
[32] H.M. Liang, C.M. Liao, Modeling VOC-odor exposure risk in livestock buildings, Chemosphere 68 (2007) 781–789.
[33] R. Wottrich, S. Diabate, H.F. Krug, Biological effects of ultrafine model particles in human macrophages and epithelial cells in mono- and co-culture, Int. J. Hyg. Environ. Health 207 (2004) 353–361.
[34] Y.K. Win, S. Feng, Effects of particle size and surface coating on cellular uptake of polymeric nanoparticles for oral delivery of anticancer drugs, Biomaterials 26 (2005) 2713–2722.
[35] D.B. Warheit, T.R. Webb, C.M. Sayes, V.L. Colvin, K.L. Reed, Pulmonary instillation studies with nanoscale TiO_2 rods and dots in rats: toxicity is not dependent upon particle size and surface area, Toxicol. Sci. 9 (2006) 227–236.
[36] H. Suzuki, T. Toyooka, Y. Ibuki, Simple and easy methods to evaluate uptake potential of nanoparticles in mammalian cells using a flow cytometric light scatter analysis, Environ. Sci. Technol. 41 (2007) 3018–3024.
[37] A. Nel, T. Xia, L. Mädler, N. Li, Toxic potential of materials at the nanolevel, Science 311 (2006) 622–627.
[38] K. Unfried, C. Albrecht, L.O. Klotz, A.V. Mikecz, S. Grether-Beck, R.P.E. Schins, Cellular responses to nanoparticles: target structures and mechanisms, Nanotoxicology 1 (2007) 52–71.
[39] D.B. Warheit, K.L. Reed, T.R. Webb, Pulmonary toxicology studies in rats with triethoxyoctylane (OTES)-coated, pigment-grade titanium dioxide particles: bridging studies to predict inhalation hazard, Exp. Lung Res. 29 (2003) 593–606.
[40] H. Arami, M. Mazloumi, R. Khalifehzadeh, S.K. Sadrnezhaad, Sonochemical preparation of TiO_2 nanoparticles, Mater. Lett. 61 (2007) 4559–4561.
[41] D. Höhr, Y. Steinfartz, R.P.F. Schins, A.M. Knaapen, G. Martra, B. Fubini, P.J.A. Borm, The surface area rather than the surface coating determines the acute inflammatory response after instillation of fine and ultrafine TiO_2 in the rat, Int. J. Hyg. Environ. Health 205 (2002) 239–244.
[42] L.C. Renwick, D. Brown, A. Clouter, K. Donaldson, Increased inflammation and altered macrophage chemotactic responses caused by two ultrafine particle types, Occup. Environ. Med. 61 (2006) 442–447.